Research Square

Preprints are preliminary reports that have not undergone peer review.
They should not be considered conclusive, used to inform clinical practice,
or referenced by the media as validated information.

# UCHL1 promotes lung cancer progression by stabilizing YAP1 and reprogramming ceramide metabolism

**Pan Chen**

chenpan08@csu.edu.cn

Hunan Cancer Hospital https://orcid.org/0000-0002-0182-2909

**Dan Wang**

Third Xiangya Hospital, Central South University

**Haixia Zhang**

Third Xiangya Hospital, Central South University

**Wenqi He**

The Third Xiangya Hospital of Central South University

**Yaqi Liao**

Hunan Cancer Hospital

**Jing He**

Third Xiangya Hospital, Central South University

**Hui Wang**

Central South University https://orcid.org/0009-0001-7693-7073

**Minghua Yang**

The Third Xiangya Hospital, Central South University https://orcid.org/0000-0002-3946-6305

**Wenjun Yin**

The Affiliated Changsha Central Hospital

**Article**

**Keywords:** lung cancer, UCHL1, YAP1, ceramide metabolism, deubiquitination, tumor progression, lipid metabolic reprogramming

**Posted Date:** June 25th, 2026

**DOI:** https://doi.org/10.21203/rs.3.rs-10022995/v1

**License:** This work is licensed under a Creative Commons Attribution 4.0 International License.
Read Full License

**Additional Declarations:** (Not answered)

# Abstract

Lung cancer remains a leading cause of cancer-related mortality worldwide, yet the molecular mechanisms driving its progression remain incompletely understood. Here, analysis of the GSE31210 dataset identified UCHL1 as a markedly upregulated deubiquitinase in lung cancer. Its high expression was validated in TCGA cohorts, clinical tissues, and lung cancer cell lines, and was associated with poor prognosis. Functional assays showed that UCHL1 promoted lung cancer cell proliferation, migration, invasion, and tumor growth in vivo.

Mechanistically, UCHL1 interacted with YAP1 and stabilized YAP1 protein by reducing its ubiquitination without affecting YAP1 mRNA expression. YAP1 restoration significantly reversed the inhibitory effects of UCHL1 knockdown, indicating that YAP1 is a critical downstream effector of UCHL1. Transcriptomic and untargeted lipidomic analyses further revealed that UCHL1 regulates lipid metabolism, particularly ceramide metabolism. UCHL1 silencing induced ceramide accumulation, accompanied by increased CERS4 and decreased CERK expression, whereas YAP1 restoration partially reversed these changes. Moreover, UCHL1 knockdown or pharmacological inhibition with LDN57444 significantly suppressed xenograft tumor growth.

Together, our findings identify UCHL1 as an oncogenic deubiquitinase that promotes lung cancer progression by stabilizing YAP1 and remodeling ceramide metabolism, highlighting the UCHL1–YAP1–ceramide axis as a potential therapeutic target.


# Introduction

Lung cancer remains one of the leading causes of cancer-related morbidity and mortality worldwide, characterized by high invasiveness, frequent metastasis, and therapeutic resistance[1–5]. Although advances in surgery, targeted therapy, immunotherapy, and multimodal treatment have improved clinical outcomes, the prognosis of patients with advanced lung cancer remains unsatisfactory. Therefore, identifying key molecular drivers of lung cancer progression is essential for developing new therapeutic strategies.

Deubiquitinating enzymes (DUBs) regulate protein stability and function by removing ubiquitin chains from substrate proteins and are increasingly recognized as important regulators of tumor progression and treatment response[6–14]. UCHL1, a member of the ubiquitin C-terminal hydrolase family, has been implicated in multiple cancers, but its function and underlying mechanism in lung cancer remain incompletely understood[15, 16].

YAP1, a core downstream effector of the Hippo pathway, promotes tumor cell proliferation, survival, invasion, migration, and EMT[16–18]. In addition to its canonical oncogenic roles, YAP1 has recently been linked to metabolic reprogramming, including lipid metabolism[19, 20]. However, whether YAP1 mediates the oncogenic function of UCHL1 in lung cancer remains unclear.

Lipid metabolic reprogramming is a key feature of cancer progression[21–23]. Ceramides, central bioactive molecules in sphingolipid metabolism, are closely involved in cell proliferation, apoptosis, stress responses, and cell fate regulation[24, 25]. Ceramide accumulation is generally associated with tumor growth inhibition and cell death, whereas dysregulated ceramide metabolism may contribute to malignant progression[26–32]. Whether ceramide metabolism is involved in UCHL1-driven lung cancer progression has not been determined.

In this study, we identified UCHL1 as a significantly upregulated DUB in lung cancer and found that high UCHL1 expression was associated with poor prognosis. Functionally, UCHL1 promoted lung cancer cell proliferation, invasion, migration, and tumor growth. Mechanistically, UCHL1 stabilized YAP1 through deubiquitination, and YAP1 restoration rescued the effects of UCHL1 knockdown. Transcriptomic and untargeted lipidomic analyses further revealed that UCHL1 regulated ceramide metabolism. UCHL1 knockdown induced ceramide accumulation, increased CERS4 expression, and reduced CERK expression, while these changes were reversed by YAP1 restoration. Together, our findings reveal a UCHL1–YAP1–ceramide metabolic axis that drives lung cancer progression and suggest UCHL1 as a potential therapeutic target.

## Materials and methods

# Cell Culture

Human lung cancer cell lines A549 and PC-9 were cultured in RPMI-1640 medium (Gibco, USA) supplemented with 10% fetal bovine serum (FBS, Gibco, USA), 100 IU/mL penicillin, and 100 IU/mL streptomycin. Cells were maintained at 37°C in a humidified atmosphere containing 5% $CO_2$. The medium was refreshed every 2–3 days, and cells were passaged when they reached 70%–80% confluence. All in vitro experiments were conducted using exponentially growing cells.

## Clinical Tissue Samples

This study was approved by the Institutional Review Board of Hunan Cancer Hospital (approval no. KY202634). Paraffin-embedded lung cancer tissues and paired adjacent normal lung tissues were collected from patients with pathologically confirmed lung cancer who underwent surgical resection at Hunan Cancer Hospital. None of the patients had received antitumor therapy before surgery. Fresh tumor tissues and matched adjacent normal tissues were immediately frozen in liquid nitrogen after surgical resection and stored at − 80°C for subsequent analysis.

## Drug Treatments

For MG132 (Sigma) treatment, transfected cells were incubated with 10 μM MG132 for 6 h. For cycloheximide (CHX, Sigma) treatment, transfected cells were incubated with 100 μg/mL CHX for

different durations (0, 6, 12, 18, and 24 h). Cells were then collected for subsequent western blot analysis.

## Plasmid Construction and Transfection

The coding sequences of UCHL1 and YAP1 were amplified by PCR and cloned into the pcDNA3.1 vector to generate the corresponding overexpression plasmids. For stable knockdown of UCHL1, short hairpin RNA (shRNA) sequences targeting UCHL1 were inserted into lentiviral vectors. The empty vector and non-targeting shRNA were used as negative controls. For transient transfection, cells were transfected with the indicated overexpression plasmids using Lipofectamine 3000 (Invitrogen) according to the manufacturer's instructions. Briefly, cells were seeded into 6-well plates and cultured to approximately 70%–80% confluence. Plasmid DNA was mixed with Lipofectamine 3000 and P3000 reagent in Opti-MEM medium, and the transfection complexes were then added to the cells. Cells were harvested 24–48 h after transfection for subsequent experiments. For stable transfection, lentiviruses carrying UCHL1 shRNA or the corresponding control were purchased from GeneChem Co., Ltd. Lentiviral infection was performed according to the manufacturer's protocol. Forty-eight hours after infection, cells were selected with puromycin (0.5-1 μg/mL) to establish stable cell lines. The stable cell lines were maintained in puromycin-containing medium and collected for RT-qPCR and western blotting to verify transfection efficiency and target gene expression.For rescue experiments, UCHL1-silenced cells were further transfected with the YAP1 overexpression plasmid, and cells were harvested for subsequent functional and molecular analyses.

## RT-qPCR Assay

Total cellular RNA was extracted using an RNAfast200 Kit (Cat# 220011, Fastagen, China). cDNA was synthesized using the Evo M-MLV RT Mix Kit (Cat# AG11728; Accurate Biology, China). qRT-PCR was performed using the SYBR® Green Premix Pro Taq HS qPCR Tracking Kit (Cat# AG11733, Accurate Biology, China), following the manufacturer's instructions. All primers used for qRT-PCR are listed in Supplementary Table S1.

# Western Blot Assay

Cells were collected by centrifugation and lysed on ice using RIPA buffer supplemented with PMSF. After high-speed centrifugation, the supernatant was collected, and protein concentrations were measured using the Pierce™ BCA Protein Assay Kit (Cat# 23225, Thermofisher, USA). Proteins were separated using polyacrylamide gel electrophoresis and transferred onto PVDF membranes. Membranes were blocked with 5% skim milk for 1 hour at room temperature, then incubated overnight with primary antibodies at 4°C. The next day, the membranes were incubated with HRP-conjugated goat anti-rabbit/mouse IgG (H + L) secondary antibodies for 1 hour at room temperature. All antibodies used are

listed in Supplementary Table S2. Protein signals were detected using the ChampChemi imaging system (SINSAGE, China).

## Immunofluorescence and Confocal Microscopy

Adherent cells were fixed in 4% paraformaldehyde for 15 minutes and permeabilized with 0.5% Triton X-100 for 10 minutes. Blocking was done with 1% BSA in PBS for 1 hour at room temperature. Primary antibodies (listed in Supplementary Table S2) were applied and incubated overnight at 4°C. The next day, cells were washed and incubated with secondary antibodies for 1 hour at room temperature. Nuclei were stained with 4',6-diamidino-2-phenylindole (DAPI, Sigma) for 5 minutes. Coverslips were mounted to prevent quenching, and fluorescence images were obtained using a confocal scanning microscope (LSM880 with Fast Airyscan, ZEISS).

## Mass Spectrometry (MS) and Co-Immunoprecipitation (co-IP) Assays

For the co-IP assay, cells were lysed on ice using IP lysis buffer and sonicated. The total protein lysate was incubated overnight at 4°C with 3 μg of specific antibodies for IP. The immune complexes were combined with Pierce™ Protein A/G Magnetic Beads (Thermo Scientific) and washed with IP wash buffer. The isolated immune complexes were separated by SDS-PAGE and visualized by Coomassie blue staining. MS was performed using Baipu Biotechnology (China). Target proteins from the co-IP were identified using western blot analysis. The antibodies used are listed in Supplementary Table S2.

# Cell Viability Assay

Cells were seeded into 96-well plates at a density of 1500 cells per well. To assess treatment effects on cell growth and viability, 10 μl of Cell Counting Kit-8 reagent was added on days 0, 1, 2, 3, and 4. After a 2-hour incubation at 37°C, absorbance was measured at 560 nm using a microplate reader, with results expressed as OD values.

# Clonogenic Assay

For colony formation assays, 500 A549 or PC-9 cells from the indicated groups were seeded into 6-well plates. The culture medium was refreshed every 3 days, and the cells were maintained for 9 days. At the endpoint, colonies were fixed with cold methanol for 30 min and stained with 0.01% crystal violet for 20 min. Plates were then photographed, and colonies were counted or quantified based on the colony-covered area per well.

# Transwell Invasion Assay

Cell migration and invasion were assessed using 24-well Transwell chambers (Corning, USA). For migration assays, 5 × 10^4 A549 or PC-9 cells from the indicated groups were suspended in serum-free

RPMI-1640 medium and seeded into the upper chambers. For invasion assays, the upper chambers were precoated with Matrigel (BD Biosciences, USA), and 5 × 10^4 cells in serum-free medium were seeded into the inserts. In both assays, the lower chambers were filled with RPMI-1640 medium containing 10% FBS as a chemoattractant. After incubation for 24 h at 37°C in a humidified atmosphere with 5% $CO_2$, cells remaining on the upper surface of the membrane were gently removed with a cotton swab. Cells that had migrated or invaded through the membrane were fixed, stained with 0.01% crystal violet, photographed under a microscope, and manually counted in at least five random fields.

# Wound-Healing Assay

For wound-healing assays, A549 or PC-9 cells from the indicated groups were seeded into 6-well plates and cultured until reaching approximately 80% confluence. A straight scratch was made across the cell monolayer using a sterile pipette tip. Detached cells were removed by washing with PBS, and the cells were then maintained in serum-free RPMI-1640 medium. Images of the wound area were captured at 0 h and 24 h under an inverted microscope. The wound closure rate was quantified using ImageJ software.

# Mouse Models

All animal experiments were approved by the Animal Ethics Committee of Hunan Cancer Hospital (no. KYJJ-2022-304) and performed in accordance with institutional guidelines.

For the in vivo tumor growth assay, A549 cells from the Ctrl, UCHL1 sh, and UCHL1 sh + YAP1 groups were collected and resuspended in culture medium containing 80% Matrigel. A total of 1 × 10^6 cells in 100 μL suspension were subcutaneously injected into mice to establish xenograft tumors. Tumor size was measured every 3 days, and tumor volume was calculated using the following formula: (length × width × height)/2. At the experimental endpoint, mice were sacrificed, and xenograft tumors were excised, photographed, weighed, and collected for subsequent histological and immunohistochemical analyses.

For pharmacological inhibition studies, 1 × 10^6 A549 cells were resuspended in culture medium containing 80% Matrigel and subcutaneously injected into mice to establish xenograft tumors. When the average tumor volume reached 30–50 $mm^3$, mice were randomly assigned to either the vehicle control (DMSO) group or the LDN-57444-treated group. Mice in the treatment group received LDN-57444 (TargetMol, T1924) dissolved in corn oil at a dose of 5 mg/kg by intraperitoneal injection once daily, whereas mice in the control group received an equal volume of vehicle. Tumor volume and body weight were recorded every 3 days. At the endpoint, tumors were harvested, photographed, and weighed. In addition, the heart, liver, spleen, lung, and kidney were collected for histological examination to assess the safety of LDN-57444 treatment.

# IHC and Hematoxylin and Eosin (HE) Staining

Tissue sections were deparaffinized, rehydrated, and treated with H2O2 to block the endogenous peroxidase activity. For IHC, sections were blocked with goat serum (Beyotime) and incubated with primary antibodies overnight at 4°C. After washing, biotinylated secondary antibodies were added,

followed by incubation with HRP-conjugated streptavidin. Diaminobenzidine (Sigma) was used for chromogenic detection and hematoxylin was used for counterstaining. For HE staining, sections were stained with hematoxylin for nuclear visualization, followed by eosin staining for cytoplasmic structures. Images were captured using the AxioVision Rel.4.6 system (Carl Zeiss). The antibodies used are listed in Supplementary Table S2.

## Statistical analysis

SPSS version 19.0 (IBM Corp., Armonk, NY, USA) and GraphPad Prism software were applied in the statistical analysis. The statistical tests for data analysis included the $\chi 2$ test, two-tailed Student's t test, log-rank test, Spearman-rank correlation test, and one-way or two way ANOVA. Data are expressed as the mean ± SD. Sig nificant difference was defined by *$p \leq 0.05$, **$p \leq 0.01$, ***$p \leq 0.001$, and ****$p \leq 0.0001$

# Results

## Identification of UCHL1 as a Potential Oncogenic Deubiquitinase in Lung Cancer

To systematically identify deubiquitinases potentially involved in lung cancer progression, we first curated a panel of 90 deubiquitinases reported in the literature and analyzed their expression profiles in the lung cancer dataset GSE31210. Among all candidate deubiquitinases, UCHL1 exhibited the most significant differential expression (Fig. 1A), suggesting that it may play an important role in lung cancer progression.

To further evaluate the clinical relevance of UCHL1 in lung cancer, we analyzed its expression pattern and prognostic value in the TCGA cohort. The results showed that UCHL1 expression was markedly elevated in lung cancer tissues compared with normal tissues (Fig. 1B), and that high UCHL1 expression was significantly associated with poor prognosis in patients with lung cancer (Fig. 1C). These findings indicate that UCHL1 may represent an important deubiquitinase involved in lung cancer development and progression.

We next validated these observations at both the cellular and clinical sample levels. Compared with the normal bronchial epithelial cell line BEAS-2B, UCHL1 was consistently upregulated in multiple lung cancer cell lines (Fig. 1D). In addition, analysis of lung cancer tissues and paired adjacent normal tissues further confirmed that UCHL1 expression was significantly higher in tumor tissues (Fig. 1E-F). Collectively, evidence from public datasets, lung cancer cell lines, and clinical specimens consistently demonstrated that UCHL1 is aberrantly upregulated in lung cancer and is closely associated with unfavorable clinical outcomes, suggesting that it may function as a tumor-promoting deubiquitinase in lung cancer.

## UCHL1 promotes lung cancer cell proliferation, invasion, and migration

Based on the above findings, we hypothesized that UCHL1, as a key deubiquitinase, may play an important role in lung cancer progression. To test this hypothesis, we established stable UCHL1-knockdown cell lines in A549 and PC-9 cells and confirmed the silencing efficiency by western blotting (Fig. 2A). Functional assays showed that depletion of UCHL1 significantly suppressed cell proliferation, as determined by the CCK-8 assay, and markedly reduced clonogenic capacity in both cell lines (Figs. 2B and 2C). In addition, Transwell invasion and wound-healing assays demonstrated that UCHL1 knockdown significantly impaired the invasive and migratory abilities of lung cancer cells (Figs. 2D and 2E). Consistently, western blot analysis revealed that silencing UCHL1 increased the expression of the epithelial marker E-cadherin while decreasing the mesenchymal marker Snail (Fig. 2F), suggesting that UCHL1 may promote malignant progression partly through regulation of EMT-related programs. Conversely, enforced expression of UCHL1 in Calu-1 cells significantly enhanced cell proliferation, colony formation, invasion, and migration (Fig. S1A–D). Consistent with these phenotypic changes, UCHL1 overexpression decreased E-cadherin expression and increased Snail expression (Fig. S1E). Together, these results demonstrate that UCHL1 promotes lung cancer cell proliferation, invasion, and migration, supporting its potential role as a tumor-promoting deubiquitinase in lung cancer.

# UCHL1 interacts with and stabilizes YAP1 by reducing its ubiquitination

To explore the molecular mechanism by which UCHL1 functions as a deubiquitinase in lung cancer, we performed immunoprecipitation followed by mass spectrometry (IP-MS) to identify potential UCHL1-interacting proteins. Among the candidates, YAP1 was identified as a prominent UCHL1-binding protein (Fig. 3A). Given that YAP1 is a key effector of the Hippo pathway and plays critical roles in cell proliferation, migration, and invasion, this finding suggested that UCHL1 may regulate malignant phenotypes in lung cancer through its interaction with YAP1.

To validate this interaction, we performed co-immunoprecipitation (Co-IP) and immunofluorescence assays. The results confirmed an exogenous interaction between UCHL1 and YAP1 (Figs. 3B and 3C). We next examined whether UCHL1 affects YAP1 expression. Notably, overexpression of UCHL1 significantly increased the protein level of YAP1, whereas its mRNA level remained unchanged (Figs. 3D and 3E), indicating that UCHL1 regulates YAP1 at the post-translational level.

Based on these observations, we hypothesized that UCHL1 stabilizes YAP1 through deubiquitination. To test this, we assessed the effect of UCHL1 on the half-life of endogenous YAP1 using a cycloheximide (CHX) chase assay. Overexpression of UCHL1 markedly prolonged the half-life of YAP1, whereas silencing UCHL1 accelerated YAP1 degradation (Figs. 3F and 3G, and Fig. S2A-B). Furthermore, ubiquitination assays showed that UCHL1 overexpression decreased the ubiquitination level of YAP1, while UCHL1 knockdown increased YAP1 ubiquitination (Fig. 3H). Together, these results demonstrate that UCHL1 interacts with YAP1 and enhances its stability by reducing YAP1 ubiquitination, thereby providing a mechanistic basis for the oncogenic role of UCHL1 in lung cancer.

# YAP1 mediates the tumor-promoting effects of UCHL1 in lung cancer cells

To determine whether YAP1 mediates the oncogenic effects of UCHL1 in lung cancer, we established UCHL1-stable knockdown cells and subsequently restored YAP1 expression in this background. The expression levels of UCHL1 and YAP1 were confirmed by western blotting (Fig. 4A). We then examined the malignant phenotypes of cells under different treatments. Functional assays showed that UCHL1 knockdown markedly suppressed the proliferation of lung cancer cells, whereas re-expression of YAP1 significantly reversed this inhibitory effect (Fig. 4B). Similarly, silencing UCHL1 significantly impaired colony-forming ability, while restoration of YAP1 partially rescued clonogenic growth (Fig. 4C).

Further functional analyses demonstrated that UCHL1 depletion significantly reduced the invasive and migratory capacities of lung cancer cells. Importantly, re-expression of YAP1 in UCHL1-silenced cells markedly restored both invasion and migration (Figs. 4D and 4E). Collectively, these findings indicate that YAP1 restoration effectively rescues the tumor-suppressive phenotypes caused by UCHL1 depletion, supporting the notion that YAP1 acts as a critical downstream functional effector of UCHL1 in lung cancer progression.

# UCHL1 promotes lung cancer progression through YAP1-dependent ceramide metabolic remodeling

Given that the above results demonstrated that UCHL1 promotes lung cancer cell proliferation, invasion, and migration by stabilizing YAP1 through deubiquitination, we next investigated whether the UCHL1–YAP1 axis also contributes to lung cancer progression through lipid metabolic reprogramming. To this end, LUAD tumor samples from the TCGA dataset were stratified into UCHL1-high and UCHL1-low groups according to the median expression level of UCHL1 (Fig. 5A). Differential expression analysis followed by GO enrichment analysis showed that genes associated with UCHL1 expression were significantly enriched in lipid metabolism-related biological processes (Fig. 5B), suggesting that UCHL1 may participate in the regulation of lipid metabolism in lung cancer.

Based on this observation, we further performed untargeted lipidomic profiling in Ctrl, UCHL1 sh, and UCHL1 sh + YAP1 cells to systematically evaluate the impact of the UCHL1–YAP1 axis on the lipid metabolic landscape. Among all differential lipid classes identified in pairwise comparisons, ceramides (Cer) consistently represented the most significantly altered lipid subclass and exhibited the largest number of differential lipid species (Fig. 5C), indicating that ceramide metabolism may be a key downstream event in UCHL1–YAP1-mediated lipid remodeling.

Further analysis revealed that UCHL1 knockdown markedly promoted ceramide accumulation, with Cer 36:2;O2|Cer 18:2;O2/18:0 showing the most prominent increase (Fig. 5D). Since elevated ceramide levels are generally associated with suppressed proliferation and restrained malignant progression, these findings, together with the inhibitory effects of UCHL1 depletion on cell proliferation, invasion, and

migration, suggest that UCHL1 may maintain malignant phenotypes in lung cancer at least partly by suppressing ceramide accumulation. Considering that ceramide abundance is coordinately regulated by both its synthesis and metabolism, we next examined the expression of key enzymes involved in ceramide homeostasis. The results showed that silencing UCHL1 significantly increased the expression of the ceramide synthase CERS4 while decreasing the expression of the ceramide kinase CERK. Notably, these changes were markedly reversed by YAP1 re-expression in UCHL1-silenced cells (Figs. 5E and 5F). Collectively, these results indicate that UCHL1 promotes lung cancer progression, at least in part, through YAP1-dependent ceramide metabolic remodeling.

# Targeting UCHL1 suppresses lung cancer growth in vivo

To further evaluate the role of the UCHL1-YAP1 axis in lung cancer growth in vivo, we established subcutaneous xenograft models using Ctrl, UCHL1-stable knockdown, and UCHL1 knockdown plus YAP1 re-expression lung cancer cells. Compared with the Ctrl group, UCHL1 depletion markedly suppressed xenograft tumor growth, whereas re-expression of YAP1 in the UCHL1-silenced background substantially reversed this inhibitory effect. Tumor growth curves and endpoint tumor weight measurements consistently showed that UCHL1 knockdown significantly reduced tumor volume and weight, while YAP1 restoration partially rescued the in vivo tumor growth capacity (Figs. 6A–C).

To determine whether the UCHL1-YAP1 axis also mediates the molecular alterations observed in vitro, we performed immunohistochemical (IHC) analysis on xenograft tissues. The results showed that UCHL1 knockdown markedly reduced the expression of YAP1 and the proliferation marker Ki-67, while increasing the expression of the ceramide synthesis-related enzyme CERS4 and decreasing the expression of the ceramide metabolism-related enzyme CERK. Notably, these changes were largely reversed by YAP1 re-expression in UCHL1-depleted tumors (Fig. 6D). These findings are consistent with our in vitro data and further support that UCHL1 promotes lung cancer growth through YAP1-dependent regulation of proliferation and ceramide-associated metabolic molecules.

To further assess the therapeutic potential of targeting UCHL1 in vivo, tumor-bearing mice were treated with the UCHL1 inhibitor LDN-57444, with DMSO as the vehicle control. Compared with the DMSO group, LDN-57444 treatment significantly suppressed tumor growth, as evidenced by reduced tumor volume and tumor weight (Figs. 6E–G). Moreover, IHC analysis showed that Ki-67 expression was markedly decreased in the LDN-57444-treated tumors, indicating reduced proliferative activity (Fig. 6H). In addition, H&E staining of major organs revealed no obvious histological damage in the heart, liver, spleen, lung, or kidney, suggesting that LDN-57444 exhibited no overt toxicity under the experimental conditions (Fig. S3A).

Together, these results demonstrate that UCHL1 promotes lung cancer growth in vivo in a YAP1-dependent manner and is accompanied by alterations in ceramide metabolism-related molecules. More importantly, pharmacological inhibition of UCHL1 effectively suppresses tumor progression in vivo, supporting the potential of UCHL1 as a therapeutic target in lung cancer.

# Discussion

Lung cancer remains one of the leading causes of cancer-related mortality worldwide. Its high invasiveness, metastatic potential, and therapeutic resistance continue to contribute to poor clinical outcomes. Although substantial advances have been made in targeted therapy, immunotherapy, and multimodal treatment strategies, the molecular mechanisms underlying lung cancer progression remain incompletely understood. Therefore, identifying novel key drivers and actionable therapeutic targets remains of great importance. As integral components of the ubiquitin regulatory network, deubiquitinases (DUBs) modulate the stability, localization, and function of substrate proteins and are broadly involved in tumor cell proliferation, migration, invasion, and treatment response. Elucidating the roles of specific DUBs and their downstream mechanisms in lung cancer may therefore deepen our understanding of its molecular pathogenesis and provide new opportunities for therapeutic intervention.

In the present study, we identified UCHL1 from a panel of 90 DUBs and demonstrated that it is highly expressed in lung cancer tissues, lung cancer cell lines, and public datasets, with elevated expression significantly associated with poor patient prognosis. Functional assays further showed that UCHL1 depletion markedly inhibited lung cancer cell proliferation, invasion, and migration, whereas UCHL1 overexpression exerted the opposite effects. These findings indicate that UCHL1 primarily functions as a tumor-promoting DUB in lung cancer. Notably, the role of UCHL1 appears to be highly context dependent, with tumor-suppressive functions reported in certain cancer types and oncogenic functions observed in others. Our data support a predominantly oncogenic role for UCHL1 in lung cancer and suggest that its aberrant upregulation may represent an important molecular basis for maintaining malignant phenotypes.

To further elucidate the mechanism by which UCHL1 drives lung cancer progression, we performed IP-MS and identified YAP1 as a UCHL1-interacting protein. As a core effector of the Hippo pathway, YAP1 is widely recognized as a critical transcriptional co-activator that promotes cell proliferation, migration, invasion, and EMT in multiple malignancies, and its aberrant activation has been closely linked to aggressive behavior in lung cancer. In this study, the interaction between UCHL1 and YAP1 was validated by Co-IP and immunofluorescence assays. We further showed that UCHL1 overexpression increased YAP1 protein levels without affecting its mRNA expression, indicating post-transcriptional regulation. Combined CHX chase and ubiquitination assays demonstrated that UCHL1 prolongs the half-life of YAP1 by reducing its ubiquitination, thereby stabilizing YAP1 protein. More importantly, rescue experiments showed that re-expression of YAP1 significantly reversed the inhibitory effects of UCHL1 depletion on proliferation, colony formation, invasion, and migration. Together, these findings establish YAP1 as a critical downstream effector of UCHL1 and identify the UCHL1–YAP1 axis as an important driver of lung cancer progression.

Metabolic reprogramming has increasingly been recognized as a hallmark of tumor progression, and lipid metabolic abnormalities are particularly important for membrane biosynthesis, signal transduction, oxidative stress adaptation, and cell fate regulation. Notably, accumulating evidence suggests that YAP1

not only functions as a canonical transcriptional regulator but also participates in metabolic remodeling. However, the mechanisms by which DUBs regulate lipid metabolism through Hippo/YAP1 signaling remain poorly understood. In the present study, analysis of TCGA-LUAD data revealed that genes associated with high UCHL1 expression were significantly enriched in lipid metabolism-related biological processes, suggesting a potential role for UCHL1 in lipid metabolic regulation in lung cancer. Subsequent untargeted lipidomic profiling showed that ceramides were the most prominently altered lipid subclass, and UCHL1 knockdown markedly promoted ceramide accumulation, which was partially reversed by YAP1 re-expression. These findings indicate that the UCHL1–YAP1 axis not only regulates malignant phenotypes such as proliferation and migration, but may also sustain tumor progression through remodeling of lipid metabolism, particularly ceramide metabolism.

Ceramides are central bioactive lipids within the sphingolipid network and play important roles in regulating proliferation, apoptosis, stress responses, and cell fate determination. In many settings, ceramide accumulation is associated with restrained tumor growth, enhanced cell death, and suppression of malignant progression. Accordingly, the marked increase in ceramide levels observed after UCHL1 knockdown was highly consistent with the reduced proliferative, invasive, and migratory capacities of lung cancer cells. Mechanistically, we further found that silencing UCHL1 increased the expression of the ceramide synthesis-related enzyme CERS4 while decreasing the expression of the ceramide metabolism-related enzyme CERK, and these changes were substantially reversed by YAP1 restoration. These results suggest that UCHL1 may coordinately regulate key enzymes involved in ceramide synthesis and metabolism in a YAP1-dependent manner, thereby suppressing ceramide accumulation and maintaining a pro-tumorigenic lipid state in lung cancer cells. In other words, UCHL1 not only promotes classical malignant phenotypes through stabilization of YAP1, but may also help sustain a metabolic environment favorable for tumor growth and invasion by limiting the accumulation of ceramide, a lipid mediator with tumor-suppressive potential.

Our in vivo experiments further supported this model. UCHL1 knockdown significantly suppressed xenograft tumor growth, while YAP1 re-expression partially rescued this effect, confirming the importance of the UCHL1–YAP1 axis in lung cancer progression in vivo. Immunohistochemical analysis showed that UCHL1 depletion reduced YAP1 and Ki-67 expression, while increasing CERS4 and decreasing CERK, which was consistent with our in vitro findings. This concordance between in vitro and in vivo data strengthens the reliability of the proposed mechanism. Moreover, pharmacological inhibition of UCHL1 using LDN-57444 significantly suppressed xenograft growth and reduced Ki-67 expression without causing obvious organ toxicity. These results suggest that targeting UCHL1 is not only mechanistically rational but also of potential translational relevance. Given the persistent challenges of recurrence and therapeutic resistance in lung cancer, UCHL1 may represent a promising target with both biological and therapeutic significance.

Several limitations of this study should be acknowledged. First, the functional role of UCHL1 was mainly validated in lung cancer cell lines and subcutaneous xenograft models, and its generalizability across additional molecular subtypes and larger clinical cohorts requires further investigation. Second, although

we demonstrated that UCHL1 stabilizes YAP1 and influences ceramide metabolism, the precise ubiquitin linkage types involved and the deeper molecular basis of ceramide metabolic remodeling remain to be fully elucidated. Further mechanistic and clinical studies will therefore be needed to better define the translational potential of the UCHL1–YAP1–ceramide axis.

In summary, we propose a novel mechanistic model in which UCHL1 stabilizes YAP1 through deubiquitination, thereby promoting lung cancer cell proliferation, invasion, and migration. At the same time, the UCHL1–YAP1 axis suppresses ceramide accumulation and remodels ceramide-associated metabolic regulators, thereby further sustaining malignant progression. Pharmacological inhibition of UCHL1 effectively restrains tumor growth in vivo. These findings not only expand our understanding of the role of DUBs in lung cancer progression, but also highlight the UCHL1–YAP1–ceramide metabolic axis as a potential therapeutic strategy for lung cancer.

## Conclusion

In conclusion, our study demonstrates that UCHL1 is aberrantly upregulated in lung cancer and is associated with poor prognosis. Mechanistically, UCHL1 stabilizes YAP1 through deubiquitination, thereby promoting lung cancer cell proliferation, invasion, migration, and tumor growth in vivo. Furthermore, the UCHL1-YAP1 axis sustains malignant progression by suppressing ceramide accumulation and remodeling ceramide-associated metabolic regulators. Importantly, pharmacological inhibition of UCHL1 effectively suppresses tumor growth in vivo. These findings identify the UCHL1-YAP1-ceramide axis as a critical mechanism underlying lung cancer progression and suggest that targeting this pathway may represent a promising therapeutic strategy for lung cancer.

## Declarations

# Ethics approval and consent to participate

The study was conducted in accordance with the guidelines approved by the Institutional Review Board of Hunan Cancer Hospital (no. KYJJ-2022-304). All participants provided written informed consent.

# Consent for publication

Not applicable.

# Data availability

The public gene expression dataset used in this study is available in the Gene Expression Omnibus (GEO) database under accession number GSE31210. All other data supporting the findings of this study

are included in the article and its supplementary information, or are available from the corresponding author upon reasonable request.

# Competing interests

The authors declare that they have no competing interests.

# Funding

This work was supported by grants from the National Natural Science Foundation of China (No. 82173201, 82272758, 82270185), the Natural Science Foundation of Hunan Province (No.2025JJ20099, 2026JJ30186) , Hunan Provincial Science and Technology Innovation Platform and Talent Program (No.2022RC3077), Health Research Project of Hunan Provincial Health Commission (No.20256687), the Key Research and Development Program of Hunan Province (No.2024DK2007), the Hunan Provincial Science and Technology Department(No.2023ZJ1125), and the Wisdom Accumulation and Talent Cultivation Project of the Third Xiangya Hospital of Central South University.

# Author Contributions Statement

D.W. and H.X.Z. contributed equally to this work. M.H.Y., P.C., and W.J.Y. conceived and designed the study. D.W., H.X.Z., W.Q.H., Y.Q.L., and L.Y. contributed to data collection, data organization, and manuscript drafting. D.W., H.X.Z., W.Q.H., Y.Q.L., H.J., and H.W. contributed to data analysis and interpretation. D.W. and H.X.Z. prepared the figures. D.W., H.X.Z., H.W., M.H.Y., P.C., and W.J.Y. revised and edited the manuscript. M.H.Y., P.C., and W.J.Y. supervised the study. All authors have read and approved the submitted version of the manuscript.

# Acknowledgements

Not applicable

# Author information

1 The Affiliated Cancer Hospital of Xiangya School of Medicine, Central South University/Hunan Cancer Hospital, Changsha, China
Dan Wang, Haixia Zhang, Yaqi Liao, Hui Wang, Pan Chen

2 Department of Pediatrics, Third Xiangya Hospital, Central South University, Changsha, China
Dan Wang, Haixia Zhang, He Jing, Minghua Yang

3 Department of Clinical Laboratory Medicine, The Affiliated Changsha Central Hospital, Hengyang Medical School, University of South China, Changsha, China
Wenqi He, Wenjun Yin

# References

1. Bray, F., et al., *Global cancer statistics 2022: GLOBOCAN estimates of incidence and mortality worldwide for 36 cancers in 185 countries*. CA Cancer J Clin, 2024. 74(3): p. 229–263.
2. Xie, S., et al., *The metastasizing mechanisms of lung cancer: Recent advances and therapeutic challenges*. Biomed Pharmacother, 2021. 138: p. 111450.
3. Xi, Z., et al., *Traditional Chinese medicine in lung cancer treatment*. Mol Cancer, 2025. 24(1): p. 57.
4. Huang, Q., et al., *Advances in molecular pathology and therapy of non-small cell lung cancer*. Signal Transduct Target Ther, 2025. 10(1): p. 186.
5. Onder, L., et al., *Fibroblastic reticular cells generate protective intratumoral T cell environments in lung cancer*. Cell, 2025. 188(2): p. 430–446.e20.
6. Liu, F., et al., *Ubiquitination and deubiquitination in cancer: from mechanisms to novel therapeutic approaches*. Mol Cancer, 2024. 23(1): p. 148.
7. Liu, J., et al., *Deubiquitylase USP52 Promotes Bladder Cancer Progression by Modulating Ferroptosis through Stabilizing SLC7A11/xCT*. Adv Sci (Weinh), 2024. 11(45): p. e2403995.
8. Chen, L., et al., *USP13 facilitates a ferroptosis-to-autophagy switch by activation of the NFE2L2/NRF2-SQSTM1/p62-KEAP1 axis dependent on the KRAS signaling pathway*. Autophagy, 2025. 21(3): p. 565–582.
9. Zhang, M., et al., *USP20 deubiquitinates and stabilizes the reticulophagy receptor RETREG1/FAM134B to drive reticulophagy*. Autophagy, 2024. 20(8): p. 1780–1797.
10. Qiao, Q., et al., *USP28 promotes tumor progression and glycolysis by stabilizing PKM2/Hif1-α in cholangiocarcinoma*. Cell Oncol (Dordr), 2024. 47(6): p. 2217–2231.
11. Xu, X., et al., *USP21 deubiquitinates and stabilizes HSP90 and ENO1 to promote aerobic glycolysis and proliferation in cholangiocarcinoma*. Int J Biol Sci, 2024. 20(4): p. 1492–1508.
12. Bian, S., et al., *Ubiquitin-specific protease 1 facilitates hepatocellular carcinoma progression by modulating mitochondrial fission and metabolic reprogramming via cyclin-dependent kinase 5 stabilization*. Cell Death Differ, 2024. 31(9): p. 1202–1218.
13. Zhang, H., et al., *Combining decitabine with radiotherapy to enhance nasopharyngeal carcinoma radiosensitivity via the TFAP2C-OTUD1-SLC25A11 axis*. Cell Death Dis, 2025. 16(1): p. 525.
14. Zhang, D., et al., *USP10 Inhibits Ferroptosis via Deubiquinating POLR2A in Head and Neck Squamous Cell Carcinoma*. Adv Sci (Weinh), 2025. 12(36): p. e12271.
15. Liu, S., et al., *UCHL1 is a potential molecular indicator and therapeutic target for neuroendocrine carcinomas*. Cell Rep Med, 2024. 5(2): p. 101381.

16. Lokman, N.A., et al., *Proteomics analysis of serum extracellular vesicle identifies UCHL1 as a potential therapeutic target for high grade serous ovarian cancer*. Br J Cancer, 2026. 134(2): p. 195–207.
17. Sadhukhan, P., et al., *YAP1 induces bladder cancer progression and promotes immune evasion through IL-6/STAT3 pathway and CXCL deregulation*. J Clin Invest, 2024. 135(2).
18. Ng, J., et al., *Molecular and Pathologic Characterization of YAP1-Expressing Small Cell Lung Cancer Cell Lines Leads to Reclassification as SMARCA4-Deficient Malignancies*. Clin Cancer Res, 2024. 30(9): p. 1846–1858.
19. Wang, S., et al., *A feedforward loop between STAT1 and YAP1 stimulates lipid biosynthesis, accelerates tumor growth, and promotes chemotherapy resistance in mutant KRAS colorectal cancer*. Commun Biol, 2025. 8(1): p. 1278.
20. Wang, J., et al., *Dietary Palmitic Acid Drives a Palmitoyltransferase ZDHHC15-YAP Feedback Loop Promoting Tumor Metastasis*. Adv Sci (Weinh), 2025. 12(6): p. e2409883.
21. Jin, H.R., et al., *Lipid metabolic reprogramming in tumor microenvironment: from mechanisms to therapeutics*. J Hematol Oncol, 2023. 16(1): p. 103.
22. Yang, K., et al., *The role of lipid metabolic reprogramming in tumor microenvironment*. Theranostics, 2023. 13(6): p. 1774–1808.
23. Gong, Z., et al., *Lipid-laden lung mesenchymal cells foster breast cancer metastasis via metabolic reprogramming of tumor cells and natural killer cells*. Cell Metab, 2022. 34(12): p. 1960–1976.e9.
24. Wang, K., et al., *Ceramide(d18:1/18:1)-NDUFA6 interaction inactivates respiratory complex I to attenuate oxidative-stress-driven pathogenesis in liver ischemia/reperfusion injury.* JCI Insight, 2025. 10(10).
25. Błachnio-Zabielska, A.U., et al., *The Interplay between Oxidative Stress and Sphingolipid Metabolism in Endometrial Cancer.* Int J Mol Sci, 2024. 25(19).
26. Wajapeyee, N., T.C. Beamon, and R. Gupta, *Roles and therapeutic targeting of ceramide metabolism in cancer*. Mol Metab, 2024. 83: p. 101936.
27. Alizadeh, J., et al., *Ceramides and ceramide synthases in cancer: Focus on apoptosis and autophagy*. Eur J Cell Biol, 2023. 102(3): p. 151337.
28. Liu, Y.Y., R.A. Hill, and Y.T. Li, *Ceramide glycosylation catalyzed by glucosylceramide synthase and cancer drug resistance*. Adv Cancer Res, 2013. 117: p. 59–89.
29. Oleinik, N.V., et al., *Ceramide-Induced Metabolic Stress Depletes Fumarate and Drives Mitophagy to Mediate Tumor Suppression*. Cancer Res, 2025. 85(17): p. 3313–3334.
30. Camacho, L., et al., *Implication of Ceramide Kinase/C1P in Cancer Development and Progression*. Cancers (Basel), 2022. 14(1).
31. Payne, A.W., et al., *Ceramide kinase promotes tumor cell survival and mammary tumor recurrence*. Cancer Res, 2014. 74(21): p. 6352–63.
32. Schwalm, S., et al., *Ceramide Kinase Is Upregulated in Metastatic Breast Cancer Cells and Contributes to Migration and Invasion by Activation of PI 3-Kinase and Akt*. Int J Mol Sci, 2020. 21(4).

# Tables

Tables 1 and 2 are available in the supplementary files section

# Figures

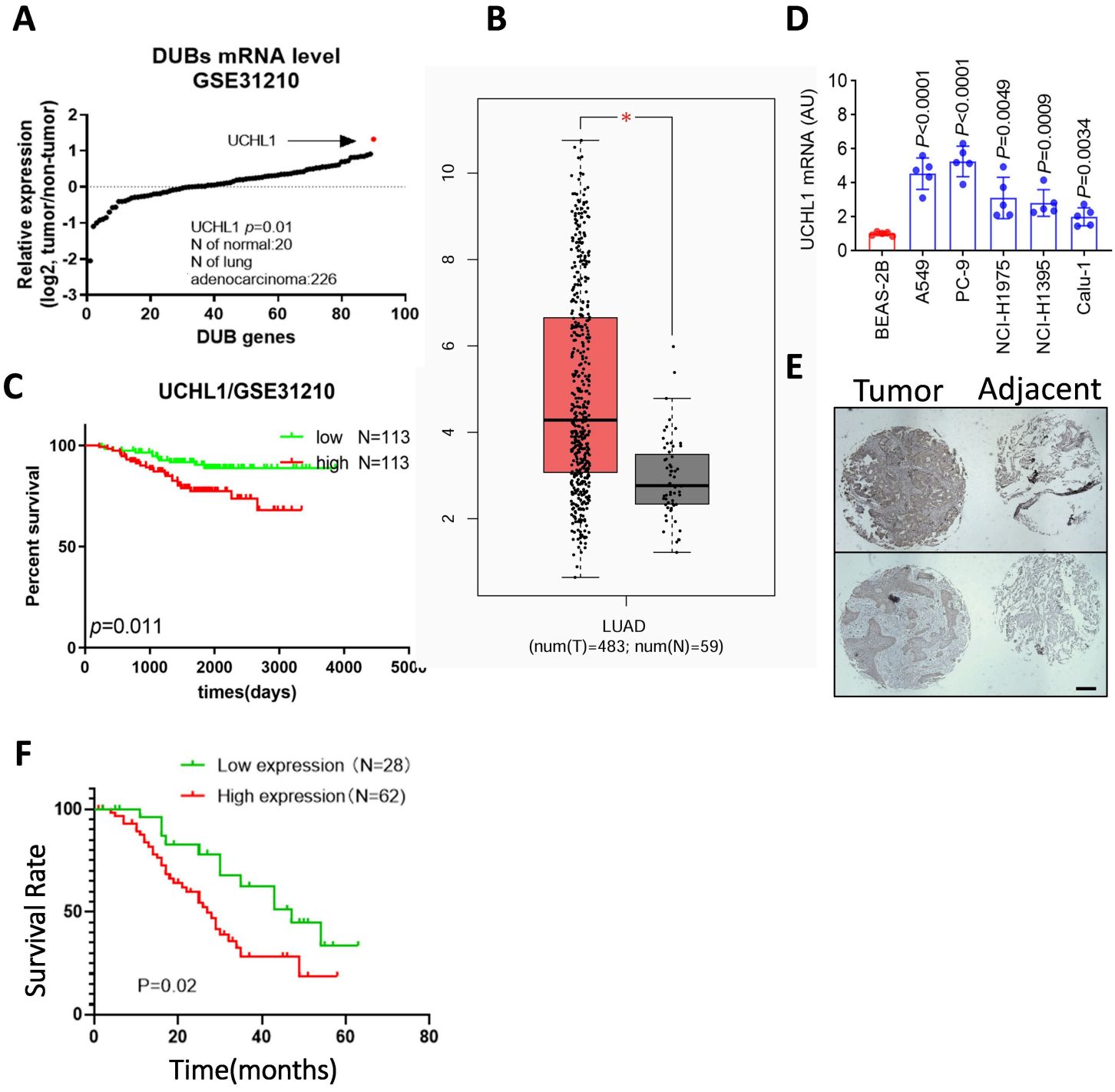



**Figure 1**

**Identification of UCHL1 as a potential oncogenic deubiquitinase in lung cancer**

(A) Expression profiling of 90 deubiquitinases in the GSE31210 lung cancer dataset identified UCHL1 as the most significantly dysregulated deubiquitinase candidate. (B) UCHL1 expression in lung cancer tissues and normal tissues from the TCGA cohort. (C) Kaplan–Meier survival analysis showing the association between UCHL1 expression and overall prognosis in patients with lung cancer from the TCGA cohort. (D) Relative expression of UCHL1 in the normal bronchial epithelial cell line BEAS-2B and the indicated lung cancer cell lines, as determined by RT-qPCR. (E) Representative images of UCHL1 expression in human lung cancer tissues and paired adjacent normal tissues, detected by immunohistochemistry. (F) Quantification of UCHL1 expression in lung cancer tissues and paired adjacent normal tissues, and analysis of the association between UCHL1 expression and patient prognosis in the clinical cohort. Data are presented as mean ± SD unless otherwise indicated. Statistical significance was determined by Student's t test, log-rank test, or the indicated statistical methods. *p < 0.05, *p < 0.01, *p < 0.001, *p < 0.0001; n.s., not significant.

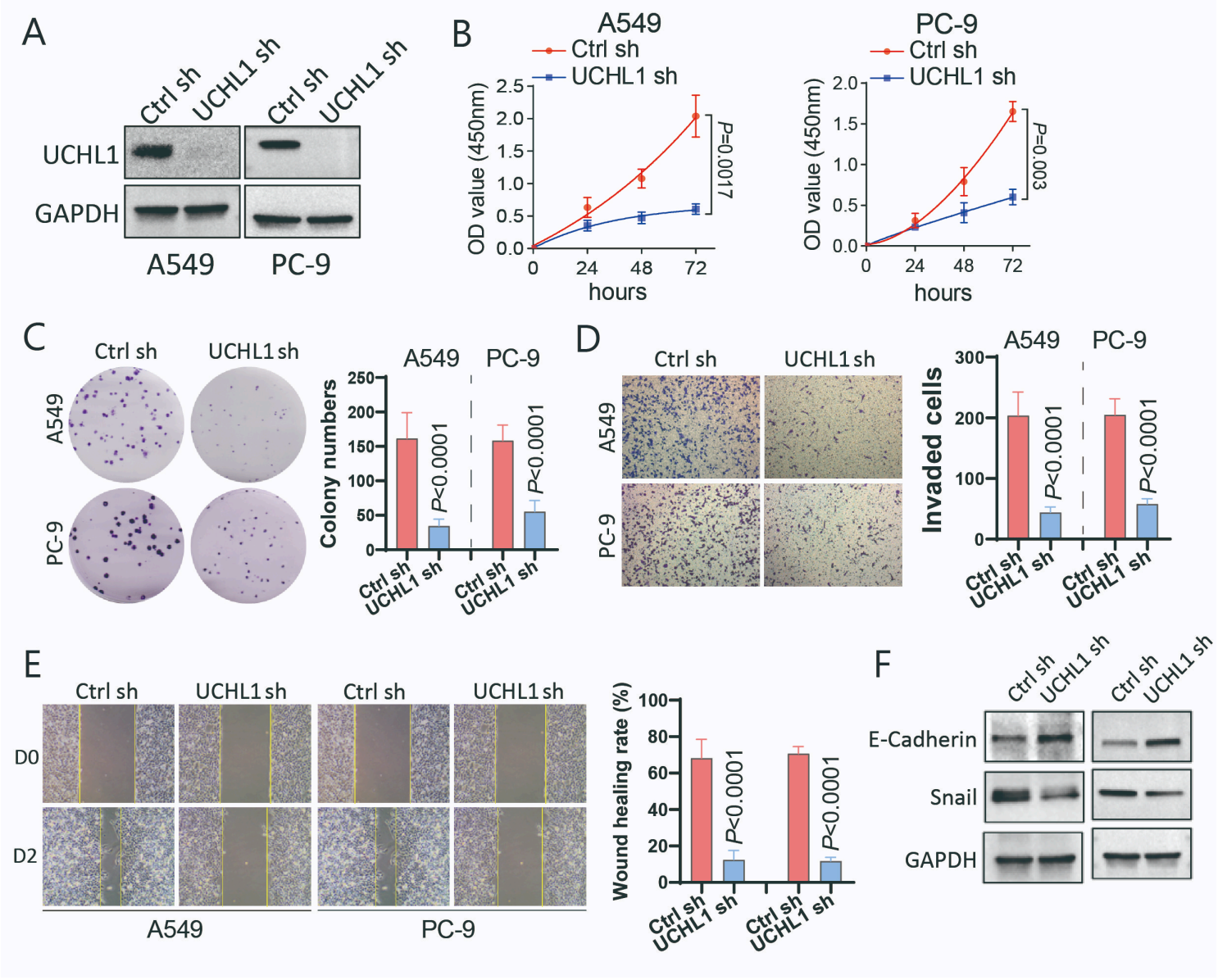
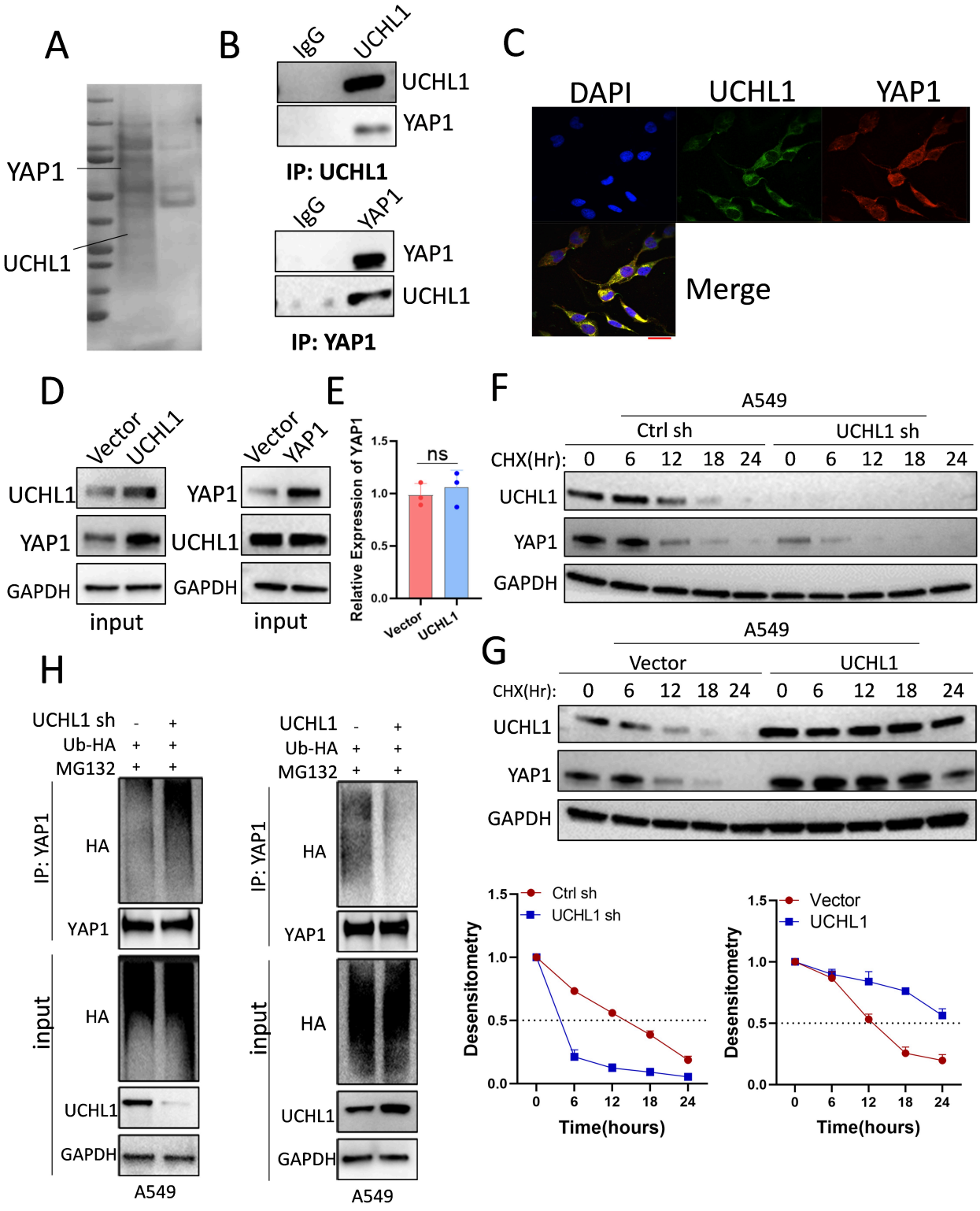


**Figure 2**

**UCHL1 promotes proliferation, invasion, and migration of lung cancer cells**

(A) Western blot analysis confirming stable knockdown of UCHL1 in A549 and PC-9 cells. (B) CCK-8 assay showing the effect of UCHL1 knockdown on the proliferation of A549 and PC-9 cells. (C) Colony formation assay showing reduced clonogenic ability in UCHL1-silenced A549 and PC-9 cells. (D) Transwell invasion assay showing that UCHL1 knockdown significantly suppresses the invasive capacity of A549 and PC-9 cells. (E) Wound-healing assay showing that UCHL1 knockdown impairs the migratory ability of A549 and PC-9 cells. (F) Western blot analysis of E-cadherin and Snail expression in A549 and PC-9 cells following UCHL1 knockdown. Data are presented as mean ± SD from three independent experiments. *p < 0.05, **p < 0.01, ***p < 0.001, ****p < 0.0001; n.s., not significant.




## Figure 3

### UCHL1 interacts with YAP1 and enhances its stability by reducing ubiquitination

(A) Identification of YAP1 as a UCHL1-interacting protein by IP-MS analysis. (B) Co-immunoprecipitation assay confirming the exogenous interaction between UCHL1 and YAP1. (C) Immunofluorescence staining showing the exogenous interaction and subcellular colocalization of UCHL1 and YAP1. (D)

Western blot analysis showing that UCHL1 overexpression increases the protein level of YAP1. (E) RT-qPCR analysis showing that UCHL1 overexpression does not significantly alter YAP1 mRNA expression. (F) CHX chase assay showing that UCHL1 overexpression prolongs the half-life of endogenous YAP1. (G) CHX chase assay showing that UCHL1 knockdown shortens the half-life of endogenous YAP1. (H) Ubiquitination assay showing that UCHL1 overexpression decreases, whereas UCHL1 knockdown increases, the ubiquitination level of YAP1. Data are presented as mean ± SD from three independent experiments unless otherwise indicated. *p < 0.05, *p < 0.01, *p < 0.001, *p < 0.0001; n.s., not significant.

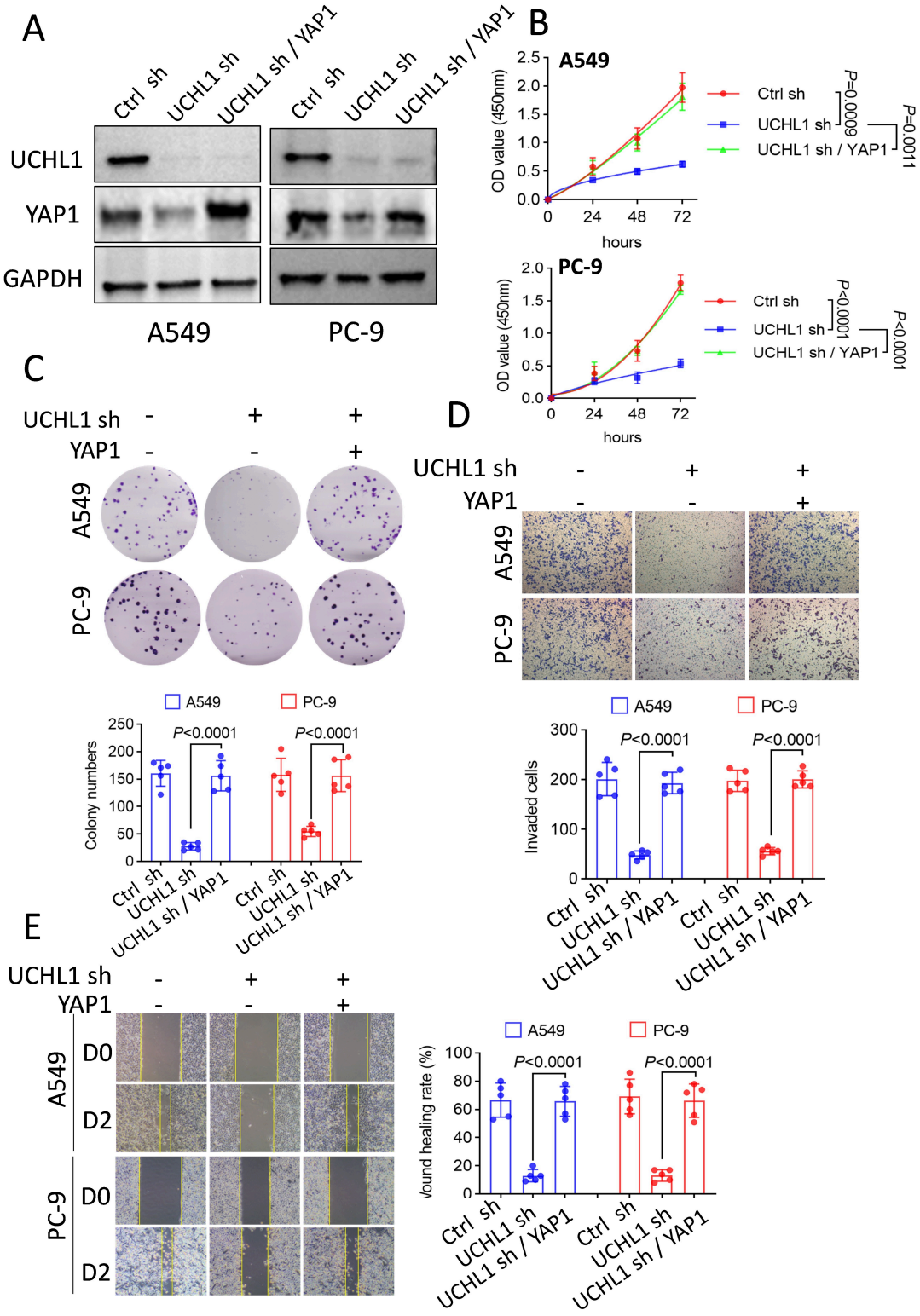
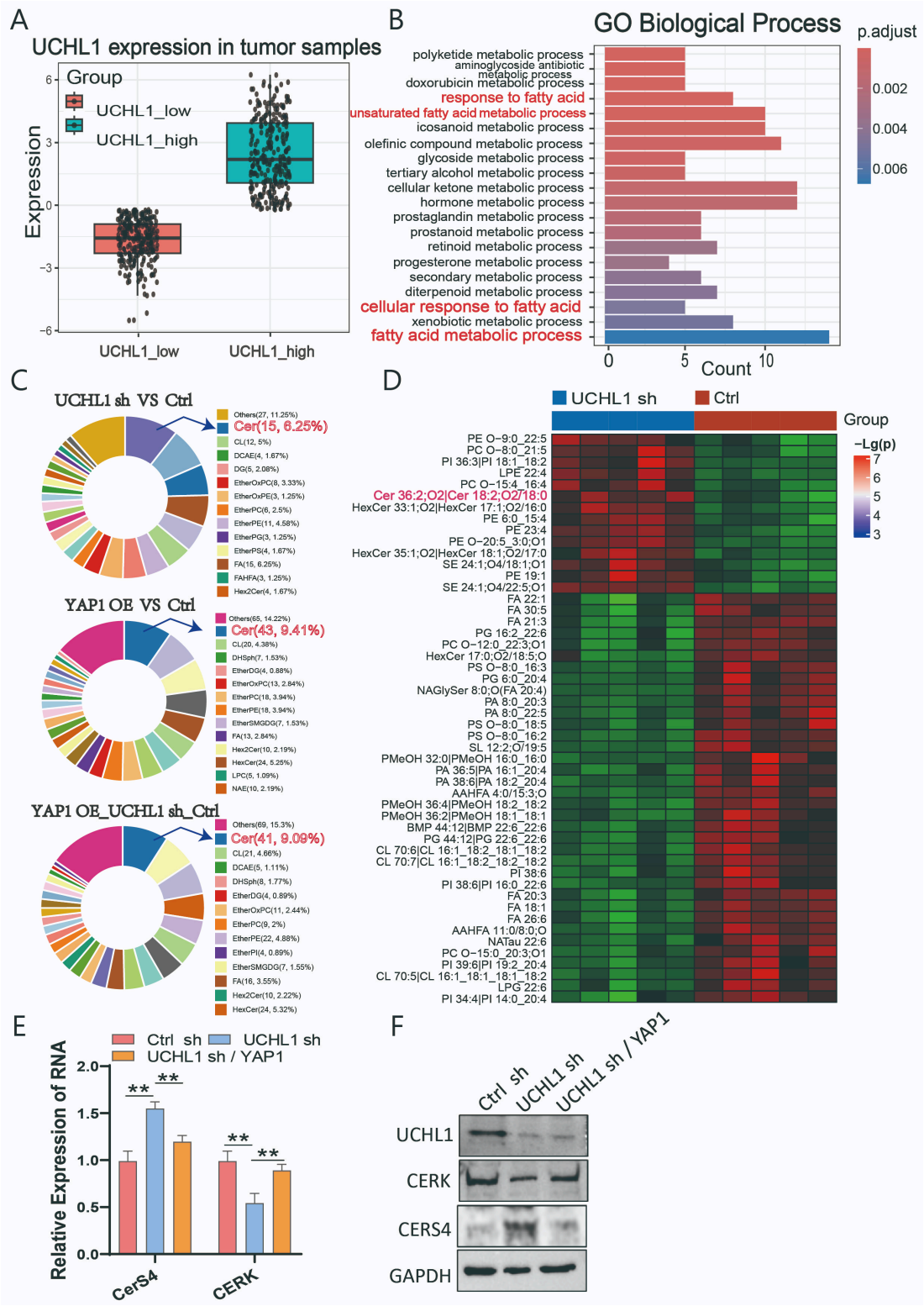


**Figure 4**

**YAP1 restoration rescues the inhibitory effects of UCHL1 depletion on malignant phenotypes in lung cancer cells**

(A) Western blot analysis confirming UCHL1 knockdown and YAP1 re-expression in the indicated lung cancer cells. (B) CCK-8 assay showing that YAP1 restoration reverses the reduced proliferative capacity caused by UCHL1 knockdown. (C) Colony formation assay showing that re-expression of YAP1 partially rescues the impaired clonogenic ability induced by UCHL1 silencing. (D) Transwell invasion assay showing that YAP1 restoration reverses the inhibitory effect of UCHL1 depletion on cell invasion. (E) Wound-healing assay showing that YAP1 restoration rescues the impaired migratory ability caused by UCHL1 knockdown. Data are presented as mean ± SD from three independent experiments. *p < 0.05, **p < 0.01*, ***p < 0.001*, *p < 0.0001; n.s., not significant.

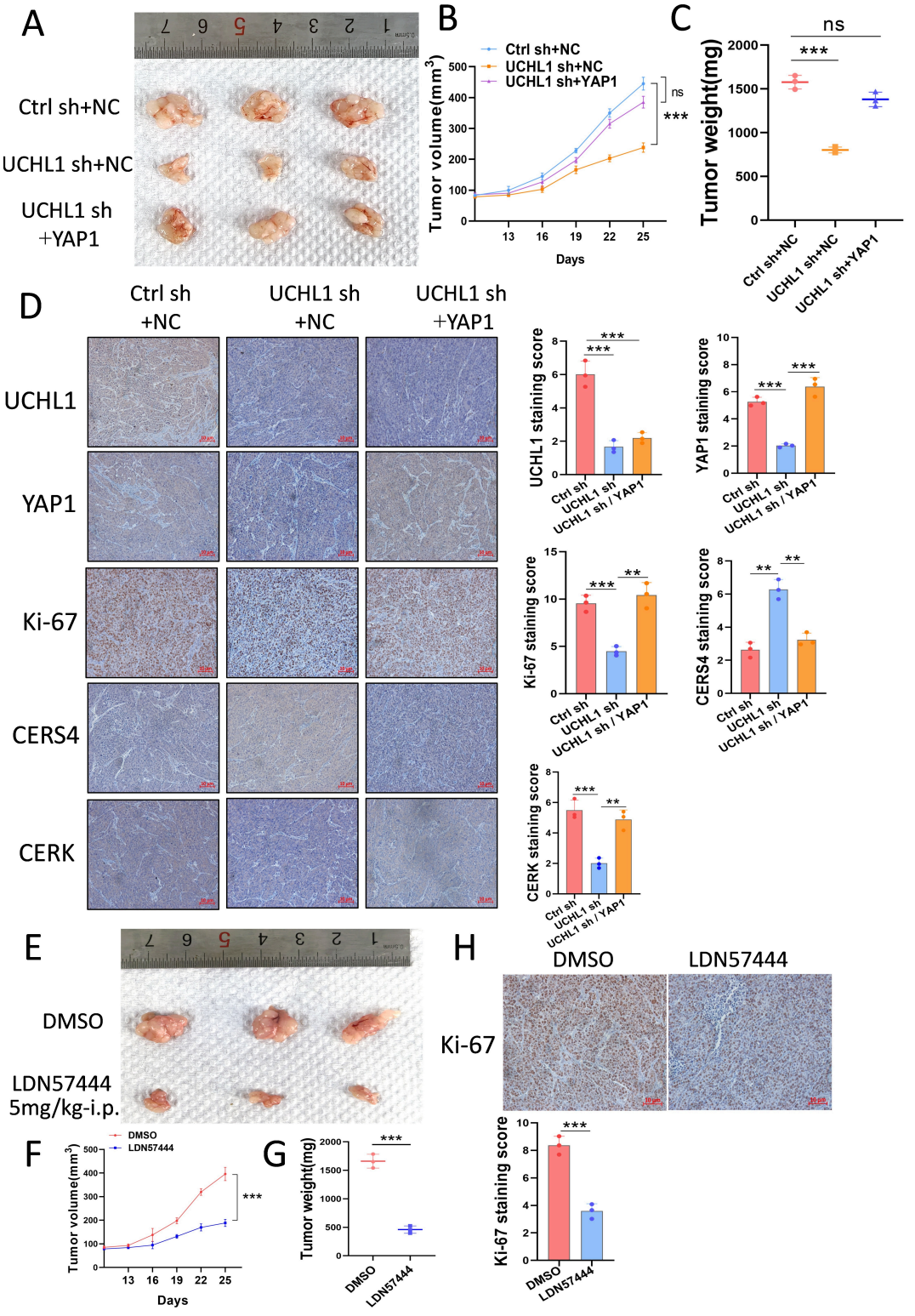



## Figure 5

### UCHL1 regulates ceramide metabolism through a YAP1-dependent manner in lung cancer cells

(A) LUAD tumor samples from the TCGA cohort were stratified into UCHL1-high and UCHL1-low groups according to the median expression level of UCHL1. (B) GO enrichment analysis of differentially expressed genes between the UCHL1-high and UCHL1-low groups showing significant enrichment of

lipid metabolism-related biological processes. (C) Untargeted lipidomic analysis of Ctrl, UCHL1 sh, and UCHL1 sh + YAP1 cells. Differential lipid class comparison showed that ceramides (Cer) represented the most significantly altered lipid subclass and contained the largest number of differential lipid species. (D) Relative abundance of ceramide species in the indicated groups, showing that UCHL1 knockdown markedly promotes ceramide accumulation, with Cer 36:2;O2|Cer 18:2;O2/18:0 displaying a prominent increase. (E) Expression analysis of the ceramide synthesis-related enzyme CERS4 in the indicated groups. (F) Expression analysis of the ceramide metabolism-related enzyme CERK in the indicated groups. Data are presented as mean ± SD from three independent experiments unless otherwise indicated. Statistical analyses were performed using the indicated methods.
*p < 0.05, *$p < 0.01$, *$p < 0.001$, *p < 0.0001; n.s., not significant.




## Figure 6

### Targeting UCHL1 suppresses lung cancer growth in vivo

(A) Representative images of xenograft tumors derived from Ctrl, UCHL1 sh, and UCHL1 sh + YAP1 cells. (B) Tumor growth curves of xenografts in the indicated groups. (C) Quantification of tumor weight at the endpoint in the indicated groups. (D) Representative IHC staining of UCHL1, YAP1, Ki-67, CERS4, and

CERK in xenograft tissues from the indicated groups. (E) Representative images of xenograft tumors from mice treated with DMSO or LDN-57444. (F) Tumor growth curves of xenografts in the DMSO and LDN-57444 treatment groups. (G) Quantification of tumor weight at the endpoint in the DMSO and LDN-57444 groups. (H) Representative IHC staining of Ki-67 in xenograft tissues from the DMSO and LDN-57444 groups. Data are presented as mean ± SD unless otherwise indicated. Statistical analyses were performed using the indicated methods. *p < 0.05, *$p < 0.01$, *$p < 0.001$, *p < 0.0001; n.s., not significant.

## Supplementary Files

This is a list of supplementary files associated with this preprint. Click to download.

- Table1primer.xlsx
- Table2antibodyanddurg.xlsx
- OriginalWesternBlots.docx
- SupplementaryMaterial.docx